# Long-wave dopplerons in tungsten and molybdenum

T. F. Butenko, V. T. Vitchinkin, A. A. Golkin, A. M. Grishin, V. A. Mishin, L. T. Tsymbal, and
A. N. Cherkasov

*Donetsk Physicotechnical Institute, Ukrainian Academy of Sciences*

We investigate theoretically and experimentally in W and Mo, at $k\|H\|[001]$, dopplerons due to carriers with the largest values (in the metals considered) of the derivative $|\partial S/\partial p_H|$. These long-wave excitations manifest themselves by resonant absorption of transverse ultrasound and by oscillations of the surface impedance of the metal plates. It is established that the long-wave dopplerons have a number of unusual properties. They depend most strongly on the inclination of the vector H to the [001] axis. The spectrum in tungsten has no threshold in weak fields, and a doppleron doublet exists in this metal in place of a single wave. The absence of a threshold and the appearance of the additional mode in W is due to the change in the sign of the nonlocal Hall conductivity for waves whose length exceeds the largest displacement of the carriers along H during the cyclotron period. The data on the doppleron-phonon resonance and on the radio-frequency size effect point to the absence of magnetic Landau damping in W and Mo at $k\|H\|[001]$, and to the onset of collisionless absorption when the magnetic field deviates from the symmetry axes by small angles of the order of 2°.

PACS numbers: 73.25. + i

We have recently published preliminary results of an investigation of doppleron-phonon resonance in W and Mo.[1] In this paper we discuss in detail the data obtained for long-wave excitations in these metals. In the first part, for a simple model of the metal ("corrugated cylinder–lens") we demonstrate the possibility of the existence of a thresholdless doppleron whose spectrum begins in weak magnetic fields. A new Fermi-surface model is proposed, namely a "truncated sphere" that describes the effects of the strong anisotropy observed in W and Mo. In the second part we present the experimental results, namely the doppleron spectra and the nonlocal conductivity in W and Mo. The mean free path and the damping length of the doppleron waves are estimated. The absence of magnetic Landau damping in the investigated metals at $k\|H\|[001]$ is proved.

## THEORY

### I. ALTERNATING CHARACTER OF THE HALL CONDUCTIVITY AND THRESHOLDLESS SPECTRUM OF THE DOPPLERON

1. It is customarily assumed that in compensated metals one of the principal distinguishing features of the dopplerons is the threshold in the wave spectrum on the side of the weak magnetic fields. In metals with a complicated Fermi surface, however, there can exist also "gapless" dopplerons, with a spectrum that begins in weak fields. Let us illustrate this statement.

The simplest properties are possessed by a doppleron that propagates along the magnetic field, $k\|H\|z$, in a compensated metal, with an axisymmetric (relative to H) Fermi surface. The dependence of the wavelength $2\pi k^{-1}$ of such an excitation on the magnetic field $H$ is determined from the dispersion equation

$$k^2 c^2 = 4\pi i \omega \sigma_{\pm}(k), \qquad (1.1)$$

where $\sigma_{\pm} = \sigma_{xx} \pm i\sigma_{yx}$ is the conductivity of the metal for a wave with circular polarization $E_{\pm} = E_x \pm iE_y \propto \exp(ikz - i\omega t)$ and frequency $\omega$. At frequencies lower than the electron relaxation frequency we have for the considered model of the metal

$$\sigma_{\pm} = \pm i \frac{n_e ec}{H} \mathscr{F}(q), \quad \mathscr{F}(q) = \sum \frac{n}{n_e} \frac{\operatorname{sgn} m}{1 \pm iv/\Omega} F\left(\frac{q}{1 \pm iv/\Omega}\right),$$

$$F(q) = \int dp_H S(1-q)^{-1} \Big/ \int dp_H S. \qquad (1.2)$$

The symbol $\Sigma$ denotes summation over all the carrier groups, $n$ is the concentration in the group, $n_e$ is the combined concentration of the electrons, $\operatorname{sgn} m$ is the sign of the cyclotron mass, $\Omega = eH/mc$ is the cyclotron frequency, $S$ is the area of the intersection of the Fermi surface with the plane $p_H = \text{const}$, $-e$ is the charge, and $p_H$ is the electron momentum along H. The dimensionless parameter of the spatial dispersion is the quantity

$$q \equiv \frac{ck}{eH} \frac{1}{2\pi} \frac{\partial S}{\partial p_H}, \qquad (1.3)$$

which is equal to the ratio of the displacement of the electron averaged over the cyclotron period to the distance between the wave fronts.

With the aid of (1.1) and (1.2) we can write down the initial relations that determine the spectrum:

$$(k')^2 = \mp 4\pi \frac{n_e e\omega}{cH} \mathscr{F}'(q) \qquad (1.4)$$

and the doppleron damping length

$$\frac{k''}{k'} = \frac{1}{2} \operatorname{sgn} \mathscr{F}' \left(\mathscr{F}' - q^2 \frac{d\mathscr{F}'}{dq^2}\right)^{-1} \sum \frac{n}{n_e} \left[ |F''| + \frac{v}{|\Omega|}\left(F' + 2q^2 \frac{dF'}{dq^2}\right)\right]. \qquad (1.5)$$

Equations (1.4) and (1.5) are valid in the case $|k''/k'| \ll 1$, where the single and double primes designate the real and imaginary parts of the quantities. From (1.5) it follows, in particular, that anomalous dispersion is possessed by dopplerons with wavelength (or $q$) such that $\operatorname{sgn}\mathscr{F}'(\mathscr{F}' - q^2 d\mathscr{F}'/dq^2) < 0$. In this case $k''/k' < 0$, i.e., the amplitude of the oscillations decreases in a direction opposite to that of the phase velocity of the wave (the vector k). In the opposite case $(k''/k' > 0)$ the doppleron has normal dispersion. The formula describes also the abrupt increase of the damping of the wave at the doppleron threshold,[2,3] where $\mathscr{F}' \approx q^2 d\mathscr{F}'/dq^2$.

2. We use now a simple two-band model. We assume

that the electron Fermi surface (the pertinent quantities are designated by the subscript 1) is a "corrugated cylinder," and the hole surface (subscript 2) consists of two parabolic cups–a "lens." According to Ref. 4

$$F_1(q_1) = (1 - q_1^2)^{-1/2}, \quad F_2(q_2) = (1 - q_2^2)^{-1},$$
$$|q_2/q_1| = \alpha = |\partial S_2/\partial p_H| / |\partial S_1/\partial p_H| < 1. \quad (1.6)$$

The function $\mathcal{F} = F_1 - F_2$ is shown in Fig. 1a. It follows from (1.6) that at $\alpha^2 \leqslant 0.5$ the summary conductivity at $q_1^2 \leqslant 1$ is always positive and the Hall current is due mainly to the electrons. If $0.5 < \alpha^2 < 1$, then for long waves ($q_1^2 < 2\alpha^{-2} - \alpha^{-4}$) the contribution of the holes to $\mathcal{F}$ predominates over the electron contribution. With decreasing wavelength, the Hall conductivity goes through zero at $q_1^2 = 2\alpha^2 - \alpha^{-4}$, and then becomes positive.

The behavior of $\mathcal{F}(q_1)$ determines completely the course of the doppleron spectrum (Figs. 1b and 1c). If $\alpha^2 < 0.5$, the spectrum has a threshold on the side of small $H$ (high energies). This is the "usual" doppleron with anomalous dispersion ($d\omega/dk \leqslant 0$, $k''/k' < 0$, dash-dot line in Fig. 1). At $\alpha^2 \geqslant 0.5$ there is no threshold. If $\mathcal{F}(q_1)$ reverses sign, then a doppleron exists in both polarizations. The additional wave in the $\oplus$ polarization is due to the section of the curve with $\mathcal{F} < 0$, and has normal dispersion over a certain interval of $k$. Figures 1b and 1c show the calculated spectra of the dopplerons for several values of the parameter $\alpha^2$. We note that even this simple model yields, depending on the value of $\alpha^2$, a set of spectral curves that differ qualitatively from one another.

Thus, the existence of a threshold in the spectrum of the doppleron wave in weak fields is due to two circumstances. First, owing to the symmetry center at small $k$ we have $\sigma_{yx}(k) \propto k^2$ (for metals with $n_e = n_h$). Second, the presence of the threshold implies a constant sign of $\sigma_{yx}$ from the very longest waves to the waves whose wavelength becomes comparable with the largest displacement (in the given metal) of the electron along $H$ over a cyclotron period. There is no threshold at small $H$ if one of these conditions is violated (for example, the
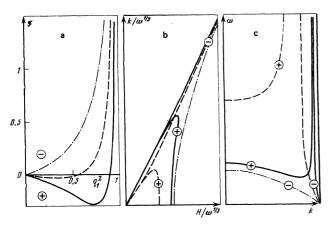
expansion of $\sigma_{yx}$ begins with higher powers of the parameter $k^2$).

3. At low frequencies, long wavelengths, and large electron mean free path:

$$\Omega \gg kv_F \gg \nu \gg \omega \quad (1.7)$$

the Hall conductivity of a compensated anisotropic metal, just as in the case of axisymmetric Fermi surface considered above, is proportional to $k^2$. This fact reflects the known Onsager relation, according to which the tensor $\hat{\sigma}$ is an even function of $\mathbf{k}$. In the case when all the orbits of the electrons in the plane perpendicular to $H$ are closed, the conductivity can be represented in the following form:

$$\sigma_{yx} = \frac{n_e e c}{H} \mathcal{F}(q_0), \quad \mathcal{F}(q_0) = A q_0^2. \quad (1.8)$$

For convenience in the comparison of the formulas with the experimental data we have introduced here the dimensionless parameter $q_0 = kcp_0/eH$, $p_0 = \hbar \cdot 1\ \text{Å}^{-1}$. The coefficient $A$ is a sum of unwieldy integrals over isolated sections of the Fermi surface, and its order of magnitude is

$$A \sim \sum \text{sgn}\, m\, \frac{n}{n_e} \left( \frac{1}{p_0} \frac{\partial S}{\partial p_H} \right)^2. \quad (1.9)$$

It contains the contributions of all the Fermi-surface sections. The increments due to the electrons and holes enter in it, as seen from (1.9), with different signs. It is therefore impossible to indicate the magnitude and the sign of the coefficient $A$ without knowing the concrete details of the Fermi surface. We have determined it for W, Mo, and Cd from experiment (see the second part).

## II. SINGULAR PART OF THE CONDUCTIVITY $\mathcal{F}(q)$

1. The form of the doppleron spectrum in strong fields, when it tends towards the straight line $q = 1$ (1.3), is determined by the character of the singularity of the Hall conductivity on this line. The form of the singularity depends on the shape of the Fermi surface near the section responsible for the doppler-shifted cyclotron resonance of the electrons with the wave. A detailed analysis of the various situations is given in Ref. 4, with a corrugated-cylinder Fermi surface as an example. In this section we consider a new model. In our opinion, it is precisely this model which describes the main regularities of long-wave dopplerons in W and Mo.

We shall assume that the "knobs" of the electron "jack" are spheres of radius $P_1$, truncated in the region of the poles $G$ (Fig. 2). If the origin is taken to be at the center of one of the spheres, then the electron dispersion law takes the form

$$\varepsilon(\mathbf{p}) = \frac{p^2}{2m}, \quad |p_z| \leqslant (P_1^2 - p_0^2)^{1/2}, \quad (2.1)$$

$p_0$ is the radius of the limiting section $G$. If the angle of inclination $\varphi$ of the vector $H$ to the symmetry axis $z$ is less than $\varphi_1 = \arcsin p_0/P_1$, then the Fermi surface has in the plane perpendicular to $H$ orbits of two types. We introduce the dimensionless momentum of the electron



FIG. 1. Nonlocal Hall conductivity (a) and doppleron spectrum [b—$k$ ($H$), c—$\omega$ ($k$)] in the "corrugated cylinder-lens" model of a metal. The dash-dot, dashed, and solid lines correspond to values of $\alpha^2$ equal to 0.2, 0.6, and 0.75, respectively. The circular polarization at which a doppleron exists is marked by the symbols $\oplus$ or $\ominus$.

along H

$$h = p_H / P_1. \tag{2.2}$$

Then, at $|h| \leqslant \cos(\varphi_1 + \varphi)$, the orbits (of type I with $|p_H| \leqslant p_1$ on Fig. 2b) pass over the spherical section of the surface and limit the circular section to the area

$$S(p_H) = \pi P_1^2 (1-h^2), \quad \frac{\partial S}{\partial p_H} = -2\pi P_1 h; \quad |h| \leqslant \cos(\varphi_1 + \varphi). \tag{2.3}$$

If $|h|$ changes from $\cos(\varphi_1 + \varphi)$ to the maximum value $|h| = \cos(\varphi_1 - \varphi)(p_1 \leqslant |p_H| \leqslant p_2$, orbits of type II on Fig. 2b), then the intersections of flat segments whose area is

$$S(p_H) = \frac{\pi}{2} P_1^2 (1-h^2) \left( 1 + \frac{2}{\pi} \eta (1-\eta^2)^{\frac{1}{2}} + \frac{2}{\pi} \arcsin \eta \right),$$

$$\cos(\varphi_1 + \varphi) \leqslant |h| \leqslant \cos(\varphi_1 - \varphi),$$
$$\eta = (\cos\varphi_1 - |h| \cos\varphi) \sin^{-1}\varphi (1-h^2)^{-\frac{1}{2}}. \tag{2.3'}$$

Henceforth, when comparing the formulas with experiment, we shall deal only with small angles

$$\varphi \ll \varphi_1. \tag{2.4}$$

We shall therefore not stop to investigate here the model at $\varphi > \varphi_1$.

2. Figure 3a shows the dependence of the derivative of the dimensionless cross section

$$\mathscr{S}(h) = S(p_H)/\pi P_1^2 \tag{2.5}$$

with respect to $h$ for several values of the angle $\varphi$ and $\varphi_1 = 45°$. The straight line $\partial \mathscr{S}/\partial h = -2h$ on the interval (2.3) corresponds to the circular orbits I. This is a spherical section of the Fermi surface. The segmental orbits (of type II) form a layer defined by the inequalities (2.3'), near each of the poles $G$. The relative thickness of the layer of these orbits is

$$\delta h = \frac{2 \sin\varphi_1 \sin\varphi}{\cos(\varphi_1 - \varphi)} \tag{2.6}$$

and amounts to approximately 30% for $\varphi_1 = 45°$ and $\varphi = 10°$. With decreasing angle $\varphi$, the thickness of the layer decreases and all the segmental orbits approach the limiting section $|h| = \cos\varphi_1$. In the layer of the segmental orbits, as seen from Fig. 3a, the quantity $\partial \mathscr{S}/\partial h$ depends nonmonotonically on $h$ and has a clearly pronounced extremum. The extremal value $|\partial \mathscr{S}/\partial h|_{extr}$ depends extremely strongly on the inclination angle $\varphi$. Figure 3b shows the dependence of this extremum on $\varphi$
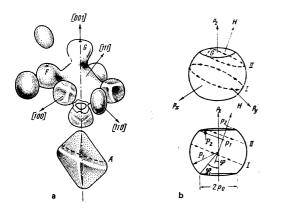
for several values of the parameter $\varphi_1$. It follows from (2.3') that at angles (2.4) the rate of change of the area (2.3') has an extremum at $|h| = \cos\varphi_1$, equal to

$$\frac{\partial \mathscr{S}_{extr}}{\partial h} = -\text{sgn } h \frac{2 \sin\varphi_1}{\pi\varphi}. \tag{2.7}$$

At small angles (2.4) the truncated-sphere model leads to a simple expression for the singular part of $\sigma_{yx}$. We write down the Hall conductivity due only to the electrons on the segmental orbits. To this end we use Eqs. (1.2) and (2.3'), in which the difference $1 - h^2$ should be replaced in the case (2.4) by $\sin^2\varphi_1$. In the integral of (1.2) with respect to $p_H = P_1 h$ we change from integration with respect to $\eta$ from (2.3'), and obtain as a result

$$\delta\sigma_{yx} = \text{sgn } m \frac{\delta n_1 ec}{H} F(q_1), \quad \delta n_1 = \frac{P_1^3 \sin^3\varphi_1}{2\pi^2 h^3} \varphi,$$

$$F(q_1) = \frac{1}{q_1 (1-q_1^2)^{\frac{1}{2}}} \text{arctg} \frac{q_1}{(1-q_1^2)^{\frac{1}{2}}}, \quad q_1 = \frac{ckP_1}{eH} \frac{\sin\varphi_1}{\pi\varphi}. \tag{2.8}$$

In these equations $\delta n_1$ is the concentration of the electrons having segmental orbits, and $q_1$ is the parameter (1.3) for the electrons with extremal values of the derivative (2.7). On the one hand, the presence of an extremum $\partial S/\partial p_H$ in the layer of the segmental orbits yields a "strong" singularity of the Hall conductivity. $F(q_1)$ has as $q_1 \to 1$ a square-root singularity $F = (\pi/2) \times (1 - q_\perp^2)^{-1/2}$ of the same type as in the corrugated-cylinder model (1.6). On the other hand, the coefficient of $F(q_1)$ in $\delta\sigma_{yx}$ is small to the extent that the layer of the segmental orbits is narrow ($\delta n_1 \propto \varphi$). If it is also recognized that the electrons on the segmental orbits can have in this metal a small displacement along H over the cyclotron period [owing to $|\partial S/\partial p_H| \propto \varphi^{-1}$ in (2.7)], then we can formulate the following conclusions. The electromagnetic properties of the metal having a group of carriers with a Fermi surface of the truncated-sphere type have a number of unusual singularities. First, the electrons on the segmental orbits give rise to the first (in the $q$-scale) Doppler-shifted cyclotron resonance of the wave. Near this resonance there should exist a doppleron mode whose spectrum has no threshold on the side of strong magnetic fields. Second, the extremal
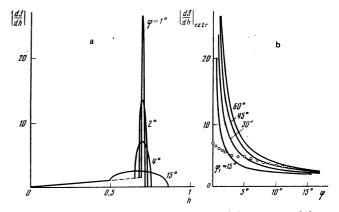
FIG. 3. a) Dependence of the derivative of the section of the Fermi surface $\mathscr{S} = S/\pi P_1^2$ on the electron momentum $h = p_H/P_1$, calculated for the model of Fig. 2b ($\varphi_1 = 45°$). b) Angular dependence of the extremal value of the derivative $|\partial \mathscr{S}(\varphi)/\partial h|$. The circles denote the results of an ultrasound experiment on Mo.

FIG. 2. a) Fermi surface of molybdenum. b) "turncated sphere" model of Fermi surface.

displacement of the "resonant" electrons depends strongly on the angle $\varphi$ between **H** and the symmetry axes. This should lead to a strong anisotropy of the long-wave doppleron spectrum. Third, in such a metal effects of weak nonlocality, due to other groups of carriers, should manifest themselves at $q_1^2 \lesssim 1$. The reson is that for a small "detuning" from the resonance $q_1^2 = 1$, such that

$$(1-q_1^2)^{1/2} > \delta n_1/n_s q_0^2 A \tag{2.9}$$

the contribution made to $\sigma_{yx}$ by the electrons on the segmental orbits turns out to be negligibly small. The estimate (2.9) follows from (1.8) and (2.8). In other words, far from the resonance the smooth function $\sigma_{yx}(q)$ is determined by all the remaining groups and can even reverse sign. The last statement is valid in the case when on the interval $0 < q_1 < 1$ the principal contribution to $\sigma_{yx}$ is made by the carriers whose sign is opposite that of the carriers with the maximum value of $|\partial S/\partial p_H|$. In this situation, as shown in Sec. I, the spectrum of the long-wave doppleron has no threshold likewise on the side of the weak magnetic field.

We note also that on the truncated sphere, the electrons on the circular orbits with $|h|$ from (2.3) cause another singularity of $\sigma_{yx}$ on top of (2.8). For these electrons it follows from (1.2) and (2.3) that

$$\delta\sigma_{yx} = \operatorname{sgn} m \frac{\delta n_2 e c}{H} F(q_2), \quad \delta n_2 = \frac{P_1^3}{6\pi^2 \hbar^3} \cos(\varphi_1+\varphi)[2+\sin^2(\varphi_1+\varphi)],$$

$$F(q) = \frac{3\cos^2(\varphi_1+\varphi)}{2+\sin^2(\varphi_1+\varphi)} \frac{1}{q^2}\left\{1+\frac{1}{2q}\left[\frac{q^2}{\cos^2(\varphi_1+\varphi)}-1\right]\ln\frac{1+q}{1-q}\right\}, \tag{2.10}$$

$$q_2 = \frac{ckP_1}{eH}\cos(\varphi_1+\varphi).$$

At $\varphi_1 \neq 0$ and as $q_2 \to 1$, the conductivity

$$F(q_2) = \frac{3}{2}\frac{\sin^2(\varphi_1+\varphi)}{2+\sin^2(\varphi_1+\varphi)}\ln\frac{1}{1-q_2}$$

diverges logarithmically. The enhancement of the singularity in comparison with the spherical Fermi surface is due to the fact that the largest displacement along **H** is made by electrons on a section of finite size.

3. The truncated Fermi-surface model (2.1) was used by us for two reasons. First, this simple model explains sufficiently fully the entire aggregate of the experimental data on Mo and W. We are unable at present to offer an alternative explanation of the results of these experiments. Second, it agrees with modern notions concerning the Fermi surfaces of Mo and W. In the Lomer model[5], which was confirmed by a calculation of the band structure of these metals in the nonrelativistic approximation, the knobs of the electron jack are spheres which are tangent at the point $G$ to the surface of the hole "octahedron" (see Fig. 2a). The spin-orbit interaction lifts the degeneracy of the energy of the carriers of the third and fourth bands, leading to a "repulsion" and deformation of the surfaces in contact. Actually the distortion of the shape of the knobs reduces, of course, not to truncation but to a gradual smoothing of the vicinity of the limiting section $G$. However, the difference between the true shape of the knob and a truncated sphere is not essential and leads only to an elimination of the singularity of $\partial \mathcal{S}_{\text{extr}}/\partial h$ from (2.7) at $\varphi = 0$.

Thus, if the flat cuts of the sphere are replaced by spherical segments of radius $P_2 > P_1$, as shown in Fig. 2b, then for the angles

$$\varphi \leqslant \varphi_2 = \arcsin p_0/P_2 \tag{2.11}$$

the derivative $|\partial\mathcal{S}/\partial h|_{\text{extr}}$ retains a constant value approximately equal to $2P_2/P_1$. The limiting part of the knob can also be non-convex.[6] Nonetheless, the proposed model is a good approximation even in this case. In fact, if the vector **H** is inclined to the symmetry axis by an angle $\varphi$ larger than the characteristic angles $\varphi_2$ of the inclination of the corrugations to the median plane, then the electron orbits differ little from the segmental ones and the dependence of $|\partial\mathcal{S}/\partial h|_{\text{extr}}$ on $\varphi$ will be similar to that shown in Fig. 3b. Deviations from the model of segmental orbits should manifest themselves at angles $\varphi < \varphi_2$ [cf. Eq. (2.11)], owing to the appearance of additional orbits on the corrugated surface of the limiting section.

We note in conclusion that the model of the truncated-sphere type is quite general and can be used to explain other kinetic phenomena with strongly anisotropic properties. For example, it can be used to explain the strong dependence of $|\partial S/\partial p_H|_{\text{extr}}$ in Mo and W at **H**$\|$[111] (Refs. 7 and 8) and in Cd.[9] In these cases the resonance effect is due to carriers from the flattened sections of the body of the hole octahedron (W and Mo) and of the "monster" Cd.

## EXPERIMENTAL RESULTS

### III. EXPERIMENTAL TECHNIQUE

The dopplerons in W and Mo were investigated by two independent experimental methods that complemented each other: doppleron-phonon resonance (DPR)[10,11] and the radiofrequency size effect (RSE).[12] The experimental technique is traditional and is described in the cited references.

The samples were cut from single crystals of W and Mo with $\rho_{300\text{ K}}/\rho_{4.2\text{ K}} = 1.5 \times 10^5$ and $6 \times 10^4$, respectively. The perpendicularity of the [001] axis to the surface of the samples was monitored with a DRON-2 x-ray apparatus. The accuracy of the **H**$\|$[001] alignment was not worse than $0.3°$. The sample rotation was accurate to about $0.1°$.

The velocity of the transverse sound $s$ was determined by the method of McScimin.[13] At $T = 4.2$ K the value of $s$ for transverse sound of arbitrary polarization, propagating in the [001] direction, is

$$s_W = (2.88\pm0.03)\times10^5 \text{ cm/sec}, \quad s_{Mo} = (3.27\pm0.03)\times10^5 \text{ cm/sec}. \tag{3.1}$$

### IV. PROCEDURE OF CONSTRUCTING THE DOPPLERON SPECTRA

1. In ultrasound investigations, the DPR manifests itself in the form of sharp maxima on the plot of the coefficient $\Gamma$ of absorption of transverse sound against the magnetic field (Fig. 4). There was no DPR for longitudinal sound. Since the DPR takes place when the wavelengths $2\pi/k$ and $2\pi s/\omega$ of the doppleron and of the sound coincide, the spectrum of the doppleron wave $k(H)$ can be easily obtained by varying $\omega$. The fact that this function is single valued is a measure advantage of the acoustic
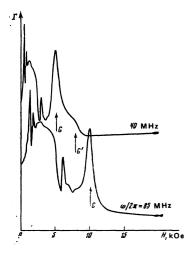
912     Sov. Phys. JETP 51(5), May 1980

Butenko *et al.*     912

FIG. 4. Typical experimental plot of the absorption coefficient
$\Gamma$ of transverse ultrasound in W ($\mathbf{k} \| [001]$, $\varphi = 2°$) against the
magnetic field $H$. The arrows $G$ and $G'$ mark the peaks of the
doppleron-phonon resonance.

method. Its main shortcoming is the impossibility of
smoothly varying the sound frequency, since resonant
converters are used.

2. In the investigations of the RSE (Fig. 5), on the
contrary, one can obtain a continuous spectrum of the
doppleron. Up to now the doppleron spectra were con-
structed by starting from the possibility of numbering
the oscillations, if the spectrum in an experiment in a
strong magnetic field falls on the asymptote $q = 1$ (1.3).
Then $k(H) = 2\pi N(H)/d$, where $d$ is the thickness of the
sample and $N$ is the number of the oscillations. On the
other hand, if the asymptotic region is not reached, then
the position of the spectrum is not defined relative to the
$k$ axis (Fig. 6).

To find the point $k = 0$ (or, equivalently, to determine
$N$) we propose the following principle. The quantities

$k$, $\omega$, and $H$ enter the dispersion equation (1.1) in the
form of the ratios $k/\omega^{1/3}$ and $H/\omega^{1/3}$. Therefore the
doppleron spectrum can be naturally specified in terms
of the coordinates $(k/\omega^{1/3}, H/\omega^{1/3})$. In terms of the co-
ordinates $(k, H)$ it breaks up into a series of spectra
corresponding to different frequencies $\omega_i$. In this case
its point $(k/\omega^{1/3})^*$, $(H/\omega^{1/3})^*$ on each $i$-th spectrum,
plotted in the coordinates $(k, H)$, corresponds to a point
$k_i = (k/\omega^{1/3})^* \omega_i^{1/3}$, $H_i = (H/\omega^{1/3})^* \omega_i^{1/3}$. It is seen that
$k_i = H_i (k/\omega^{1/3})^* (\omega^{1/3}/H)^*$, i.e., the indicated $i$-th points
lie on the straight line $k = H = 0$ passing through the
origin.

In experiment this principle is used in the following
manner. The spectrum is plotted in terms of the co-
ordinates $k$ and $H$ at a definite frequency $\omega_i$ (Fig. 6).
The frequency is then slightly changed in such a way
that the displacement of the given oscillation along $H$
(shown by the arrow in Fig. 6) is less than the distance
to the neighbors, and the spectrum is plotted for the
frequency $\omega_2$. This procedure guarantees a correct
(with respect to the number $N$) placement of the spec-
tra at the frequencies $\omega_1$ and $\omega_2$ relative to each other.
We choose on the first spectrum an arbitrary point $C_1$
corresponding to a certain value $H_1/\omega_1^{1/3}$. On the second
spectrum we find a point $C_2$ with $H_2$ such that $H_2/\omega_2^{1/3}$
$= H_1/\omega_1^{1/3}$. The straight line passing through $C_1$ and $C_2$
crosses the $k$ axis at the sought point $k = 0$, since the
condition $k_1/\omega_1^{1/3} = k_2/\omega_2^{1/3}$ should be satisfied. The $G$-
spectrum of W and Mo constructed in this manner (Fig.
7) agrees well with the results of acoustic investiga-
tions, although the oscillations are observed in mag-
netic fields far from the asymptotic region.

## V. SPECTRUM OF THE DOPPLERONS IN W, Mo, AND Cd

1. Figure 7 shows the spectra of the dopplerons in W,
Mo, and Cd. The dopplerons $A$, due to the group of
carriers near the section $A$ on the octahedron (Fig. 2a),
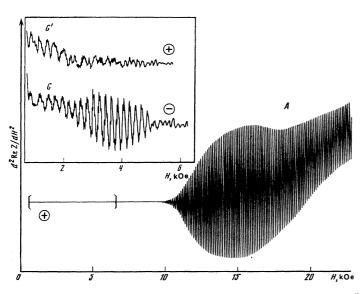manifest themselves extremely strongly both in W and



FIG. 5. Typical experimental plot of the surface impedance in W ($\mathbf{H} \| \mathbf{n} \| [100]$, $d = 1.72$ mm, $\omega/2\pi = 3.5$ MHz). The manifestation of
$A$ and $G$ dopplerons is seen. The inset shows a section of the plot marked on the main figure by square brackets, when the appa-
ratus sensitivity is increased by a factor of 200.

in Mo, in the form of oscillations of the surface impedance (Fig. 5, see also Refs. 14 and 15). The use of thick samples (large number of oscillations) and the saturation of the period in a strong magnetic field made it possible to determine with high accuracy the values

$$R_{extr} = \frac{1}{2\pi\hbar} \left| \frac{\partial S}{\partial p_H} \right|_{extr} = \begin{cases} 0.514 \pm 0.005 \, A^{-1} & \text{for} \quad \text{Mo} \\ 0.495 \pm 0.005 \, A^{-1} & \text{for} \quad \text{W} \end{cases} \quad (5.1)$$

The close values of $R_{extr}$ in W and Mo is attributed to the fact that the surface of the hole octahedron has almost the same shape and dimension. No $A$-doppleron was observed in magnetoacoustic measurements. The possible reason is that the value of $k/\omega^{1/3}$ reached in ultrasound measurements is smaller than those values of this parameter at which the $A$ doppleron is observed in the RSE experiments (Fig. 7).

2. The long-wave dopplerons $G$, on the contrary, manifest themselves strongly in the form of DPR, but lead to very weak oscillations in the RSE (see Figs. 4 and 5). In our opinion these dopplerons are due to electrons near the limiting section $G$ (Fig. 2a) of the knobs of the jack. This is indicated by the following: the large value of $R_{extr}$, which is possible, judging from the available experimental and theoretical investigations of the Fermi surface of these metals (see, e.g., Refs. 7 and 16) only for this group of electrons; the sign of the carriers that produce the effects; the angular dependence of the $G$-spectrum; and finally the satisfactory description of the resonance within the framework of the truncated-sphere model.

In contrast to the $A$ dopplerons, as seen from Figs. 7 and 8, we did not reach the asymptotic form of the $G$-doppleron spectrum. Therefore we present in place of $R_{extr}$ the value of $R_{exp}$, which was determined from the last high-frequency points on the spectra and is an upper-bound estimate of $R_{extr}$ :

$$R_{extr} \leqslant R_{exp} \begin{cases} 1.14 \pm 0.02 \, A^{-1} & \text{for} \quad \text{Mo} \\ 0.9 \pm 0.05 \, A^{-1} & \text{for} \quad \text{W} \end{cases} \quad (5.2)$$

In molybdenum, the dispersion of the spectrum [its deviation from the straight line $q = 1$ (1.3)] increases with decreasing $k/\omega^{1/3}$, which the DPR amplitude decreases. At frequencies of the order of 50 MHz, the DPR is practically indistinguishable against the background of the smooth function $\Gamma(H)$. Thus, the $G$ spectrum in Mo is a typical spectrum with a threshold in weak magnetic fields. For comparison, Fig. 7 shows the spectra of the doppleron modes in Cd, due to electrons from the vicinity of the limiting point of the
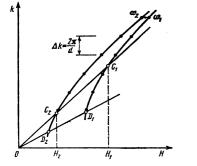
"lens"–$L$ and to carriers on the body of the "monster"–$M$.

In contrast to these excitations, the doppleron $G$-mode in W has a number of exceptional singularities. First, the spectrum of this mode has no threshold in weak magnetic fields (Fig. 7). The peak of the DPR in tungsten becomes weaker and broadens substantially both with decreasing and with increasing frequency. Second, at small $k$ (such that $k/\omega^{1/3} \leqslant 1.1$ sec$^{1/3}$ cm$^{-1}$ at $H \| [\,001\,]$) there exist in W two doppleron waves, $G$ and $G'$. In Cd $Cd(L)$, Mo($G$), and at high frequencies in W($G$) the corresponding DPR peak is the last resonant maximum, in the scale of $H$, of ultrasound absorption. In W, however, in a limited range of frequencies (18–26 MHz), on the right-hand wing (relative to $H$) of the resonance $G$-line there is observed a weak and broad additional absorption maximum $G'$ (Fig. 4). Special experimental investigations of its position have made it possible to establish that the $G$ and $G'$ peaks diverge with relative to $H$ with decreasing frequency. This was the first indication that an additional wave exists. The $G'$ spectrum is shown dashed in Fig. 7 (cf. the situation considered in Sec. I and in Fig. 1b).

3. To make the spectra more accurate and to determine the signs of the carriers that produce the long-wave mode, we used radio-frequency measurements of the surface impedance (Fig. 5). In the region where the $G$-doppleron exists, one observes in thin samples several series of oscillations due to other short-wave excitations.[14] Against their background, the $G$ oscillations are practically indistinguishable. The short-period oscillations become weaker with increasing sample thickness, $G$-dopplerons and appear on samples with thickness of the order of 2 mm. As seen from Fig. 5, the intensity of the $A$ doppleron, observed for metals in
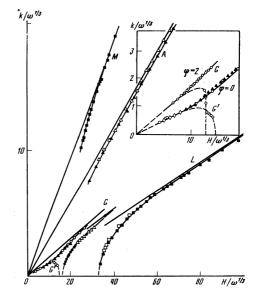
FIG. 7. Spectra of dopplerons in W, Mo, and Cd (Refs. 3 and 10). ●, □, ○—data of acoustic measurements: △, ■, ▲—RSE, ○, ▲—W, □, ■—Cd, and ●, △—Mo. Inset—angular dependence of the spectra of the dopplerons $G$ in W. The symbols ◇ correspond to oscillations of the surface resistance that exist in weak fields in both polarizations (see Fig. 5). The value of $\varphi$ is in degrees.

FIG. 6.

polarization, is approximately two or three orders of magnitude larger than the intensity of the $G$ doppleron. For molybdenum, the $G$ doppleron is observed only in $\oplus$ polarization, as is typical behavior of a wave formed by electrons, and reveals, just as in DPR, a threshold on the side of weak magnetic fields. The spectrum obtained from the radio-frequency measurements agrees with the DPR spectral curve (Fig. 7). In tungsten and at $\ominus$ polarization, in fields up to 5 kOe (Fig. 5) one can see oscillations whose spectrum agrees (see Fig. 7) with the $G$ spectrum obtained from the DPR. The additional wave manifests itself by oscillations in the $\oplus$ polarization in fields up to 2 kOe. In this field interval, the oscillations in the $\oplus$ and $\ominus$ polarizations coincide. This proves the existence of the $G'$ mode also in weak magnetic fields, where the spectra of the $G$ and $G'$ dopplerons coalesce. The $G$ and $G'$ oscillations in weak magnetic fields cannot be interpreted as the Gantmakher-Kaner effect. Although their spectrum does lie on the straight line $q_0^2 \approx 0.45$, this line does not correspond to Doppler-shifted cyclotron resonance (DSCR) of $G$ ($q_0^2 \approx 0.91$). No additional DSCR with $q_0^2 \approx 0.45$, which might cause the Gantmakher-Kaner effect, was observed in the local conductivity of tungsten.[1] Moreover, at these values of $q_0^2$, as will be shown in Sec. VI and in Fig. 8, the Hall conductivity becomes very small. Thus, the $G$ and $G'$ oscillations are due to the presence of long-wave electromagnetic excitations in W.

4. A distinguishing feature of the $G$ spectra in W and Mo is their strong anisotropy. It suffices to indicate that inclination of the magnetic field away from the [001] axis by only an angle $\varphi \sim 2°$ changes the value of $R_{exp}$ by approximately 20%. The experimental results of the angle measurements for Mo are shown in Fig. 3b. With increasing $\varphi$, the DPR in Mo becomes weaker
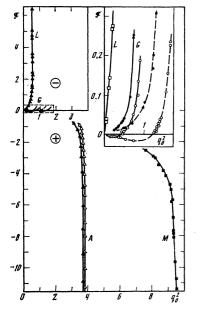


FIG. 8. Nonlocal Hall conductivity, obtained experimentally in W, Mo, and Cd. Inset—the same in the interval $q_0^2 \lesssim 2$. The dashed lines show plots of $\mathcal{F}(q_0^2)$ in Mo and W at $\varphi = 2°$. The notation is the same as in Fig. 7, with the exception of the points ▲ on the $L$ curve, which represents the RSE data for Cd.

(with exception of the angle region $\varphi \lesssim 1°$), begins at ever increasing frequencies, and at $\varphi \gtrsim 10-12°$ it becomes hardly distinguishable. The inset in Fig. 7 demonstrates the existence of a $G'$ mode in W also when H is inclined away from [001].

The function $R_{exp}(\varphi)$ for molybdenum was investigated using the experimental spectra and is shown by circles on the plot of the derivative of $|\partial\mathcal{F}/\partial h|_{extr}$ against $\varphi$ (Fig. 3b). To make $R_{exp}$ dimensionless, we used Eqs. (2.2) and (2.5), and a knob radius $P_1 = 0.34\ \hbar\ \text{Å}^{-1}$ obtained from Ref. 16. It is seen from Fig. 3b that at $\varphi \gtrsim 7°$ the experimental points fit fairly well the theoretical curve with $\varphi_1 = 45°$. This value of $\varphi_1$, in turn, agrees with the model of Ketterson et al.,[16] based on the data of the de Haas-van Alphen effect. At small angles $\varphi \lesssim 7°$, the model of the truncated sphere overestimates the result for $R_{extr}$. As already noted in Sec. II, this can be due to the corrugation of the limiting section $G$. In fact, from precision SRE experiments[6] one can obtain for the characteristic corrugation angles $\varphi_2$ of the knob $G$ the estimate $\varphi_2 \sim (7-8)°$, which agrees with our data. We emphasize once more that in the discussion of our experiments the truncated-sphere model can be used only for angles $\varphi \gtrsim \varphi_2$. At smaller inclination angles it is necessary to specify in detail the form of the limiting section $G$.

The oscillations of the surface impedance due to the $G$ doppleron, both in W and in Mo, were observed in an extremely narrow range of angles $\varphi$ (less than 1°) and could not be used for the study of the anisotropy of the spectra. As indicated at the end of the first part of this paper, the model of the truncated sphere predicts the existence of DSCR on the line $q_2 = 1$ from (2.10). This resonance is due to the sharp limit on the existence of circular orbits on the knob $G$ (the kink of $\partial\mathcal{F}/\partial h$ at $|h| = \cos(\varphi_1 + \varphi)$). The value of $R$ obtained from (2.10) with $\varphi_1 = 45°$, $\varphi = 0$, and $p_1$ from Ref. 16 turns out to be 0.24 Å$^{-1}$. A DSCR corresponding to such a value of $R$ has been experimentally observed.

## VI. RECONSTRUCTION OF THE NONLOCAL CONDUCTIVITY FROM THE DOPPLERON SPECTRA

1. The nondissipative part of the conductivity $\mathcal{F}(q_0)$ can be obtained by using the experimental plots of $k/\omega^{1/3}$ against $H/\omega^{1/3}$ and the dispersion relation (1.4) rewritten in the form

$$\mathcal{F}(q_0) = -\frac{\beta c}{4\pi n_e e}\left(\frac{k}{\omega^{1/3}}\right)^2\frac{H}{\omega^{1/3}}, \quad q_0 = 1\,\text{Å}^{-1}\frac{\hbar c}{e}\frac{k}{\omega^{1/3}}\frac{\omega^{1/3}}{H}, \qquad (6.1)$$

where $\beta$ is the sign of the polarization of the doppleron wave. The electron density $n_e$ in (6.1) was determined from the volume $V_p$ of the electron Fermi surface, $n_e = V_p/4\pi^3\hbar^3$. To calculate the volumes we used the RSE data for Cd (Ref. 17) and of the de Haas-van Alphen effect for W and Mo.[16] The following concentrations were obtained:

$$n_e = \begin{cases} 0.5\times10^{22}\ \text{cm}^{-3} & \text{for} \quad \text{Cd} \\ 1.0\times10^{22}\ \text{cm}^{-3} & \text{for} \quad \text{W} \\ 1.55\times10^{22}\ \text{cm}^{-3} & \text{for} \quad \text{Mo}^{2)} \end{cases} \qquad (6.2)$$

The function $\mathcal{F}(q_0)$ plotted in accord with (6.1) for Cd($L$, $M$), W($A$, $G$), and Mo($A$, $G$) is shown in Fig. 8. It is seen that the $\mathcal{F}(q_0)$ curve in Mo($G$) is less steep (has

a smaller slope at small $q_0^2$) than in Cd($L$). This is a reflection of a shift of the threshold field in the spectrum of the $G$-wave in Mo into the region of smaller $H$ (cf. Fig. 7). This tendency was most clearly pronounced in W, where there is no threshold at all for the G doppleron. The latter circumstance and the existence of a $G'$ wave in the polarization $\oplus$ made it possible to conclude that in W the conductivity $\mathscr{F}$ for $\varphi = 0$ vanishes at $q_0^2 \approx 0.45$ and is negative for smaller $q_0^2$. Thus, the appearance of an additional $G'$ wave is due to the "hole-like" behavior of the Hall conductivity at $q_0^2 < 0.45$. As follows from (6.1) and Fig. 8, the spectrum of the $G'$ mode, just as of the $G$-wave, has no threshold in weak fields but is bounded on the side of large $H$.

When **H** is inclined away from [001], the point where $\mathscr{F} = 0$ shifts towards shorter wavelengths. At $\varphi = 2°$ (see the inset of Fig. 8) it corresponds to a value $q_0^2 = 1.2$. When $\varphi$ changes, the slope of the $\mathscr{F}(q_0)$ curve on Fig. 8 remains practically unchanged at small $q_0^2$. This indicates a weak angular dependence of the coefficient $A$ of the expansion of the function $\mathscr{F}(q_0)$ in (1.8) in powers of $q_0^2$—a fact evident beforehand. From the data of Fig. 8 we determine the numerical values of the coefficient $A$ of (1.8):

$$A = \begin{cases} 0.93 & \text{for} \quad \text{Cd} \\ 0.03 & \text{for} \quad \text{Mo} \\ -0.03 & \text{for} \quad \text{W} \end{cases} \qquad (6.3)$$

In contrast to Cd, the contributions made to $\mathscr{F}$ in W and Mo by the electrons and holes cancel each other almost completely even for waves with $q_0^2 \sim 0.5$. The strong cancellation of the Hall currents is apparently the cause of the different behavior of the long-wave dopplerons in W and Mo. Actually, owing to the smallness of $\mathscr{F}$, even small distortions of the Fermi surface of the metal lead to relative changes of $\mathscr{F}(q_0)$ of the order of unity and even to a reversal of the sign of the Hall conductivity for long waves. One can expect also that the properties of the long-wave dopplerons in W and Mo should change substantially under pressure.

2. Experiments on DPR and RSE yielded also data that lead to a number of conclusions concerning the dissipative properties of the investigated metals. We note first that in W and Mo at **k**‖**H**‖[001] there is no collisionless absorption of the long wave—the magnetic Landau damping.[19] In fact, as shown by Kaner and Skobov, the dissipative conductivity of an anisotropic metal under conditions (1.7) is given by a sum of the following integrals:

$$\sigma_{xx} = \frac{n_e ec}{H}(B + C|q_0|),$$

$$B = \frac{c}{4\pi^2\hbar^3 n_e eH}\sum\nu\int dp_H|m|(\overline{p_x^2} + \overline{p_y^2}), \qquad (6.4)$$

$$C = \frac{1}{4\pi\hbar^3 n_e p_0}\sum\int dp_H|m|\delta(\bar{v}_H)\,(\overline{p_x v_H}^2 + \overline{p_y v_H}^2).$$

Here p is the momentum and v the velocity of the electrons, while a superior bar denotes averaging over the cyclotron period

$$\bar{\mathbf{v}} = (2\pi)^{-1}\int_0^{2\pi}d\Phi\,\mathbf{v},$$

and $\Phi = \Omega t$ is the dimensionless time of motion of the electron over the orbit in the magnetic field. The first term in $\sigma_{xx}$ is due to collisions of the electrons with the scatterers. In this term $B \sim \nu/|\Omega|$. The magnetic damping leads to the appearance of a second term in (6.4). It does not appear when the mean values $\overline{p_x v_H}$ and $\overline{p_y v_H}$ vanish identically. These situations can be realized even in metals with a complicated Fermi surface. To this end all the orbits with $\bar{v}_H = 0$ should have a rotational symmetry with respect to $H\|z$. In the absence of magnetic Landau damping the dissipative part of the conductivity turns out in the limit as $\nu \to 0$ to be vanishingly small. An anisotropic crystal then reveals the same properties as a metal with an axisymmetric Fermi surface, considered in Sec. I.

Direct proof of the absence of Landau damping in W and Mo at **k**‖**H**‖[001] is provided by estimates of the dissipative part of $\hat{\sigma}$, obtained from the experimental data, and its dependence on the angle $\varphi$ (see below). Another indirect confirmation is the small (due only to electron collisions) direct electron absorption of transverse ultrasound in Mo and W in a strong magnetic field beyond the threshold of the last Doppler-shifted cyclotron resonance (see Ref. 11 and Fig. 4). Finally, according to the accepted models of the Fermi surfaces of Mo and W (Ref. 16) (see Fig. 2a), at **H**‖[001] there are no orbits that cause magnetic damping in these metals.

3. We consider first the case $\varphi = 0$ and estimate $\sigma_{xx}$ from (6.4) for long waves. We assume that in the experimental DPR points in Mo, which correspond to the minimal values of $k/\omega^{1/3}$ on the spectra of Fig. 7 and to the minimal $q_0^2$ on the inset of Fig. 8, the right-hand part of Eq. (1.5) becomes of the order of unity. This conclusion is based on the assumption that the DPR vanishes when the doppleron damping length becomes less than the wavelength ($k''/k' \gtrsim 1$). By determining the quantities $\mathscr{F}$, $q_0^2$, and $d\mathscr{F}/dq_0^2$ that enter in (1.5) from Fig. 8, and determining $H$ from the experimental plots, we obtain for Mo a relaxation frequency $\nu \approx 1.7 \times 10^9$ sec$^{-1}$ (mean free path $l \approx 0.06$ cm). This rough estimate gives an idea of the dissipative conductivity due to the collisions ($B \sim 10^{-2}$). At $\varphi = 0$ over an interval of small $q_0^2$ ahead of the $G$ resonance the collisions of the electrons are the only source of damping of the doppleron wave. An estimate of $\nu$ from the DPR in W is difficult. Its value could be determined, just as for Mo, from the damping of the doppleron $G'$ near the threshold on the side of large $H$. However, the line of resonance with the $G'$-wave in our experiments is so weak that one cannot even speak of quantitative results.

The energy dissipation of the short waves in W and Mo at $\varphi = 0$ can be investigated with the aid of the doppleron oscillations of the surface impedance of the section $A$ (the branch of the function $\mathscr{F}(q_0)$ with $q_0^2 \approx 3.5$ on Fig. 8). The experimentally observed $A$-doppleron threshold (see the plot on Fig. 5) is determined by the condition that the damping length of the wave be comparable with the thickness of the sample, i.e., $k''/k' \sim N^{-1}$, where $N$ is the number of the oscillation. By determining the number from experiment and the threshold values of all the quantities that enter in the denominator of (1.5) from Fig. 8 we obtain
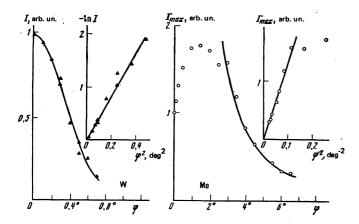
FIG. 9. Change of the amplitude $I$ of the doppleron oscillations and of the sound absorption coefficient $\Gamma$ at the maximum of the DPR when the magnetic field is inclined away from the [001] axis by an angle $\varphi$. Solid line—theoretical plots of $I(\varphi)$ from (6.10) and of $\Gamma_{max}(\varphi)$ from (6.12).

$$\mathscr{F}'' = \begin{cases} 0.72 & \text{for Mo} \\ 0.9 & \text{for W} \end{cases} \qquad (6.5)$$

This result shows that near the threshold of the $A$-doppleron the principal mechanism of the wave damping is its collisionless absorption by the electrons of group $G$ [the collisionless increments to $\mathscr{F}'' \propto \nu/|\Omega|$ turn out to be smaller by two orders than the values in (6.5)]. Far from the threshold, the role of the collisionless damping decreases greatly. As seen from (1.5), when $d\mathscr{F}'/dq^2$ increases the contribution of Im $F$ to $k''$ decreases rapidly and

$$\frac{k''}{k'} \approx -\text{sgn}\,\mathscr{F}' \frac{\nu}{|\Omega|} \frac{n}{n_e}. \qquad (6.6)$$

Near the DSCR the damping length of the doppleron wave is approximately equal to the mean free path. This conclusion is confirmed also experimentally. Under identical conditions (at fixed $\omega$ and $H$) the amplitudes of doppleron oscillations $I_1$ and $I_2$ in samples of thickness $d_1$ and $d_2$ were measured in the experiment. Since the second derivative of the surface impedance is proportional to

$$I = \text{Re}\,\frac{d^2 Z}{dH^2} \propto d^2 \exp(ikd),$$

it follows that

$$I_1/I_2 = (d_1/d_2)^2 \exp\left[-k''\,(d_1-d_2)\right]. \qquad (6.7)$$

With the aid of (6.7) we obtain from experiments on W the damping length of the doppleron $A$:

$$(k'')^{-1} = 0.18 \pm 0.02\,\text{mm}, \qquad (6.8)$$

which was practically independent of the magnetic field. According to (6.6), this result yields an upper-bound estimate of the mean free path in W ($\rho_{300K}/\rho_{4.2K} = 60\,000$)

4. When H is inclined away from [001], both DPR and RSE experiments on W and Mo reveal the appearance of magnetic Landau damping.[3] It affects most strongly the damping of the long-wave excitations. To prove directly that collisionless absorption sets in at $\varphi \neq 0$, we investigated the angular dependences of the amplitudes of the DPR in Mo and of the long-wave doppleron oscillations of the RSE in W. These results are shown in Fig. 9. It

is seen that the amplitude $I$ of the RSE varies with increasing $\varphi$ much more rapidly than the amplitude of the DPR. The reason is that the amplitude of the RSE depends exponentially on the doppleron damping length, as against the power-law dependence of the DPR amplitude.

To demonstrate this, we obtain first the dependence of $C$ from (6.4) on $\varphi$ in analogy with what was done by Kaner and Skobov[19] in the investigation of magnetic damping of helicons. When H is inclined away from $z$ (for example, towards $y$) by an angle $\varphi \ll 1$, the mean values over orbits that are symmetric about $z$ behave in first order in $\varphi$ in the following manner:

$$\overline{p_x v_H} = 0, \quad \overline{p_y v_H} = \varphi S/2\pi m.$$

In this case we have in (6.4):

$$C = \varphi^2 \varkappa, \quad \varkappa = (8\pi^2 \hbar^3 n_e p_0)^{-1} \sum S^2 \left| \frac{\partial^2 S}{\partial p_H^2} \right|^{-1}. \qquad (6.9)$$

Now, to obtain the dependence of the amplitude $I$ of the RSE on $\varphi$, we can use the first formula of (6.7), in which we must substitute $k''$ from (1.5) with $F'' = \varkappa \varphi^2 |q_0|$ from (6.9):

$$I(\varphi) \propto \exp\left(-\varphi^2 \frac{\pi \varkappa N |q_0|}{|\mathscr{F}' - q_0^2 \, d\mathscr{F}'/dq_0^2|}\right). \qquad (6.10)$$

In the RSE, the value of $I(\varphi)$ changes radically over angles $\varphi \sim 1°$, therefore $q_0$ and $\mathscr{F}'(q_0)$ in (6.10) can be regarded as weakly dependent on $\varphi$. The exponential law (6.10), as seen from Fig. 9, agrees well with experiment if the constant $\varkappa$ from (6.9) is chosen equal to 100. The unexpectedly large value of $\varkappa$ can be attributed to the following circumstance. The magnetic Landau damping is due to electrons on the extremal section $(\overline{v}_H = 0)$. If this section belongs almost to the cylindrical section of the Fermi surface, then the derivative $|\partial^2 S/\partial p_H^2|$ can turn out to be small, and the constant $\varkappa$ [see (6.9)] large. The limiting value of $\varkappa$ is restricted by the inequality

$$\varkappa \sim |\partial^2 S/\partial p_H^2|^{-1} \ll kl,$$

which justifies the use of the delta function $\delta(\overline{v}_H)$ in the last formula of (6.4).

To estimate the sound absorption at the maximum of the DPR it is necessary to use the dispersion equation for the coupled acoustic and electromagnetic oscillations. If we confine ourselves to induction interaction of the electrons with the sound, then this relation takes the form[19] (see also Ref. 21):

$$\left(k^2 - \frac{\omega^2}{s^2}\right)\left[(k^2 - k_D^2)\left(1 - \frac{k_D^2}{\sigma_{yx}}\frac{d\sigma_{yx}}{dk^2}\right) - i\frac{4\pi\omega}{c^2}\sigma_{xx}\right] = \gamma k^4, \qquad (6.11)$$

where $\gamma = H^2/4\pi\rho s^2$, $\rho$ is the density of the crystal and $k_D^2$ is the root of Eq. (1.4). In experiment for long-wave dopplerons the condition of weak coupling of the doppleron with sound was always satisfied:

$$\left(\frac{\sigma_{xx}}{\sigma_{yx}}\right)^2 \left|1 - \frac{k_D^2}{\sigma_{yx}}\frac{d\sigma_{yx}}{dk^2}\right|^{-1} \gg 4\gamma.$$

Therefore substituting in the square brackets and in the right-hand side of (6.11) $k^2 = \omega^2/s^2$, we find that at the maximum of the DPR

$$k^2 = \frac{\omega^2}{s^2}\left(1 + i\frac{\gamma\omega c^2}{4\pi s^2 \sigma_{xx}}\right),$$

and the sound absorption coefficient is equal to

$$\frac{\Gamma_{max}}{\omega} = \frac{k''s}{\omega} = \gamma \frac{\omega c^2}{8\pi s^2 \sigma_{xx}} \propto \frac{1}{(\nu/|\Omega|) + \varkappa\varphi^2|q_0|}. \qquad (6.12)$$

The result (6.12) agrees with the behavior of the experimental curve $\Gamma_{max}(\varphi)$ on Fig. 9.

---

[1] There is no corresponding value $(2\pi\hbar)^{-1}(\partial S/\partial p_H) \approx 1.5$ of the known model of the Fermi surface of W (Ref. 16).

[2] This value of the concentration in molybdenum agrees with the value of $n_e$ given in Ref. 18.

[3] The influence of the magnetic damping on the dopplerons in Cd was investigated in Ref. 20.

---

[1] A. A. Galkin, L. T. Tsymbal, T. F. Butenko, A. N. Cherkasov, and A. M. Grishin, Phys. Lett. 67A, 207 (1978).

[2] L. M. Fisher, V. V. Lavrova, V. A. Yudin, O. V. Konstantinov, and V. G. Skobov, Zh. Eksp. Teor. Fiz. 60, 759 (1971); 63, 224 (1972) [Sov. Phys. JETP 33, 410 (1971); 36, 118 (1972)].

[3] V. P. Naberezhnykh, D. E. Zherebchevskii, L. T. Tsymbal, and T. M. Yeryomenko, Solid State Commun. 11, 1529 (1972).

[4] D. S. Falk, B. Gerson, and J. F. Carolan, Phys. Rev. B 1, 406 (1970).

[5] W. M. Lomer, Proc. Phys. Soc. London 80, 489 (1962); 84, 327 (1964).

[6] V. A. Gasparov and M. H. Harutunian, Phys. Status Solidi B 93, 403 (1979).

[7] D. E. Soule and J. C. Abele, Phys. Rev. Lett. 23, 1287 (1969).

[8] L. T. Tsymbal, Yu. D. Samokhin, A. N. Cherkasov, V. T. Vitchinkin, and V. A. Mishin, Fiz. Nizk. Temp. 5, 461 (1979)

[Sov. J. Low Temp. Phys. 5, 221 (1979)].

[9] P. D. Hambourger and J. A. Marcus, Phys. Rev. B 8, 5567 (1973).

[10] L. T. Tsymbal and T. F. Butenko, Solid State Commun. 13, 633 (1973).

[11] A. A. Galkin, L. T. Tsymbal, A. M. Grishin, and T. F. Butenko, Pis'ma Zh. Eksp. Teor. Fiz. 25, 98 (1977) [JETP Lett. 25, 87 (1977)].

[12] V. F. Gantmacher, Prog. Low Temp. Phys. 5, 181 (1967).

[13] H. J. McScimin, J. Acoust. Soc. Am. 22, 413 (1950).

[14] I. M. Vitebskii, V. T. Vitchinkin, A. A. Galkin, Yu. A. Ostroukhov, O. A. Panchenko, L. T. Tsymbal, and A. N. Cherkasov, Fiz. Nizk. Temp. 1, 400 (1975) [Sov. J. Low Temp. Phys. 1, 200 (1975)].

[15] A. A. Galkin, L. T. Tsymbal, A. N. Cherkasov, and I. M. Vitebskii, Fiz. Nizk. Temp. 1, 540 (1975) [Sov. J. Low Temp. Phys. 1, 264 (1975)].

[16] J. B. Ketterson, D. D. Koelling, J. C. Shaw, and L. R. Windmiller, Phys. Rev. B 11, 1447 (1975).

[17] V. P. Naberezhnykh, A. A. Mar'yakhin, and V. L. Mel'nik, Zh. Eksp. Teor. Fiz. 52, 617 (1967) [Sov. Phys. JETP 25, 403 (1967)].

[18] V. V. Boiko, V. A. Gasparov, and I. G. Gverdtsiteli, Zh. Eksp. Teor. Fiz. 56, 489 (1969) [Sov. Phys. JETP 29, 269 (1969)].

[19] É. A. Kaner and V. G. Scobov, Adv. Phys. 17, 605 (1968).

[20] V. V. Lavrova, V. G. Skobov, L. M. Fisher, A. S. Chernov, and V. A. Yudin, Fiz. Tverd. Tela (Leningrad) 15, 2335 (1973) [Sov. Phys. Solid State 15, 1558 (1973)].

[21] S. V. Medvedev, V. G. Skobov, L. M. Fisher, and V. A. Yudin, Zh. Eksp. Teor. Fiz. 69, 2267 (1975) [Sov. Phys. JETP 42, 1152 (1975)].

Translated by J. G. Adashko

---

# Investigation of the band structure of semiconducting Bi₁₋ₓSbₓ alloys

G. A. Mironova, M. V. Sudakova, and Ya. G. Ponomarev

*Moscow State University*
(Submitted 26 July 1979)
Zh. Eksp. Teor. Fiz. 78, 1830–1851 (May 1980)

The Shubnikof–de Haas effect is investigated at helium temperatures in the semiconduting alloys $Be_{1-x}Sb_x$ ($0.08 \leq x \leq 0.12$) of both $n$ and $p$ type. It is observed that the anisotropy of the electron ($n$-type) and hole ($p$-type) Fermi surfaces at the point $L$ of the reduced Brillouin zone decreases with increasing Fermi energy $\varepsilon_F$. The difference between the anisotropic cross sections and the cyclotron masses increases simultaneously. The degree of nonspecularity of the electron and hole spectra in the direction of elongation of the equal-energy surfaces in $L$ is determined. It is observed that the ratio of the spin and orbit splittings $\gamma = \Delta_{sp}/\Delta_{orb}$ for the maximum section of the Fermi surface in $L(H\|C_2)$ approaches unity as $\varepsilon_F \to 0$. The parameters that enter in McClure's dispersion relation [J. Low Temp. Phys. 25, 527 (1976)] are calculated.

PACS numbers: 71.25.Tn, 72.20.Mg, 71.25.Hc

## INTRODUCTION

The restructuring of the energy spectrum of $Bi_{1-x}Sb_x$ with increasing $x$ is accompanied by a transition of the alloys into the superconductiing phase in a relatively narrow concentration interval $0.07 < x < 0.23$.[1] The thermal gap of the semiconducting alloys $Bi_{1-x}Sb_x$ does not exceed 25–30 meV, so that they can be classified as narrow-gap semiconductors.[1,2] According to the results of magneto-optical measurements,[3] the energy gap $\varepsilon_{gL}$ at the point $L$ of the reduced Brillouin zone vanishes at $x \approx 0.04$ as a result of the band inversion (the gap parameter of Bi is $\varepsilon_{gL} < 0$). The anomalous smallness of the direct gap $\varepsilon_{gL}$ leads to a strong nonparabolicity of the dispersion of the carriers in $L$.[4-10]

The experimental data[11] obtained for pure Bi are best